Differential Diagnosis of Nontraumatic Intracerebral Hemorrhage*

Jennifer Linn, Hartmut Brückmann[1]

Abstract
A wide variety of nontraumatic pathologies can result in intracerebral hemorrhage (ICH). Primary causes such as arterial hypertension or cerebral amyloid angiopathy can be differentiated from secondary pathologies, such as neoplasms, arterio-venous malformations, coagulopathies, hemorrhagic ischemic strokes, and cerebral venous and sinus thrombosis.
Here, the authors first provide some general information on epidemiology, clinical presentation, and imaging appearance of ICHs followed by a detailed discussion of the different underlying pathologic entities and their imaging presentation.

Key Words: Intracerebral hemorrhage · ICH · Imaging · Secondary causes · Primary causes

Clin Neuroradiol 2009;19:45–61
DOI 10.1007/s00062-009-8036-x

Differentialdiagnose nichttraumatischer intrazerebraler Blutungen

Zusammenfassung
Eine Vielzahl nichttraumatischer Pathologien kann sich mit einer intrazerebralen Blutung manifestieren. Primäre Ursachen, wie der arterielle Hypertonus und die zerebrale Amyloidangiopathie, können hierbei von sekundär ursächlichen Erkrankungen, wie z.B. Neoplasien, arteriovenösen Malformationen, Koagulopathien, ischämischen Schlaganfällen mit sekundärer Einblutung und der Sinus- und Hirnvenenthrombose, unterschieden werden.
Diese Übersichtsarbeit bietet zunächst allgemeine Informationen bezüglich Epidemiologie, des klinischen Erscheinungsbilds und bildgebender Charakteristika des Krankheitsbildes der intrazerebralen Blutung. Im Anschluss werden die einzelnen primären und sekundären Blutungsursachen detailliert dargestellt.

Schlüsselwörter: Intrazerebrale Blutung · Bildgebung · Sekundäre Ursachen · Primäre Ursachen

Introduction

Nontraumatic intra*cranial* hemorrhage can affect the different intracranial compartments: the epidural space (epidural hematoma), the subdural space (subdural hematoma), the subarachnoid space (subarachnoid hemorrhage), as well as the brain parenchyma (intra*cerebral* hemorrhage).

This review will focus on intra*cerebral* hemorrhage (ICH). A variety of underlying pathologies can result in ICH. Depending on the underlying cause, an ICH is commonly classified into either *primary* or *secondary* hemorrhage. Primary ICHs result from spontaneous rupture of small intracerebral vessels, which are compromised by either arterial hypertension or cerebral amyloid angiopathy (CAA), and account for approximately 80% of cases [1–3]. The main causes for secondary ICHs include neoplasms, arteriovenous malformations (AVMs), coagulopathies (including anticoagulation treatment), hemorrhagic ischemic strokes, and cerebral venous and sinus thrombosis (CVST).

With respect to size, intracerebral *macro*hemorrhages with diameters of > 10 mm can be distinguished from

*Dedicated to Professor Hermann Zeumer, MD, on the occasion of his 65th birthday and his retirement.

[1]Department of Neuroradiology, University Hospital Munich, Germany.

Received: September 8, 2008; revision accepted: November 8, 2008

*micro*hemorrhages with diameters of < 10 mm. Intracerebral microbleeds typically occur in patients with arterial hypertension or CAA and tend to be multiple [4–6].

In this review, we first provide some general information on epidemiology, clinical presentation, and imaging appearance of ICHs followed by a detailed discussion of the different underlying pathologic entities. Table 1 summarizes the most important pathologies associated with primary or secondary ICH.

Table 1. Important causes of primary and secondary intracerebral hemorrhages.

Primary causes
Arterial hypertension
Cerebral amyloid angiopathy (CAA)
Secondary causes
Cerebral venous and sinus thrombosis (CVST)
• Sinus thrombosis
• Deep cerebral venous thrombosis
• Cortical venous thrombosis
Hemorrhagic ischemic stroke
Intracranial neoplasms
• Primary intracerebral tumors
• Metastases
Intracranial vascular malformations
• Arteriovenous malformations (AVMs)
• Dural arteriovenous fistulas (DAVFs)
• Cavernous malformations/cavernomas (± developmental anomalies)
Coagulopathies
• Congenital bleeding disorders
• Coagulopathic liver disease
• Neoplastic coagulopathies
• Thrombocytopenia
• Drug-induced coagulopathy

Epidemiology

Spontaneous ICHs acount for 10–15% of all strokes and are associated with a higher mortality rate compared to ischemic strokes: about 25% of all patients with hypertensive ICH die within the first 24 h.

Although ICH is found in all ethnic groups, African Americans and Japanese are more commonly affected than Caucasian people. In a population-based study in the greater Cincinnati area, the incidence of ICH was 15 per 100,000 individuals (compared to 50 cases per 100,000 African Americans and 55 cases per 100,000 Japanese people) [1]. All age groups may be affected, but the risk increases with age.

Clinical Presentation

The clinical presentation depends predominately on the size and the localization of the hemorrhage. Patients typically show an acute focal neurologic deterioration, accompanied by headache, vomiting, altered consciousness, seizures, and increased blood pressure [1, 2, 7].

Risk Factors

Increased age and arterial hypertension represent the most important risk factors for ICH. Further independent risk factors include moderate and heavy alcohol abuse, male sex, and anticoagulant treatment [1, 8–10]. Conventional anticoagulation therapy has been shown to increase the risk of ICH seven- to tenfold [11]. While cigarette smoking is more commonly associated with subarachnoid than with ICH [9], the opposite is true for diabetes mellitus [12].

The apolipoprotein ε4 genotype is associated with CAA and is known to increase the risk of recurrent lobar ICHs [13].

Imaging Characteristics

Computed Tomography

In most clinical departments, unenhanced computed tomography (CT) still remains the major imaging modality of choice in any emergency settings. Thus, it plays a major role in the detection of acute ICHs. On CT, an acute ICH typically presents as a hyperdense mass within the brain parenchyma showing Hounsfield Units (HU) of 50–70 (Figure 1). Care has to be taken in patients presenting with low hemoglobin values (< 8–10 g/dl) or bleeding diatheses, because the clot might present isodense to the brain parenchyma in such instances. In case of underlying coagulopathies or thrombolytic therapy, fluid-fluid levels can be found within the ICH on plain CT.

Within 1–6 weeks, the ICH becomes isodense (= "subacute" ICH) typically showing a decrease of attenuation of 1.5 HU a day. "Chronic" ICHs present as a hypodense mass compared to the surrounding brain parenchyma. Variable residua can be found after an ICH on CT: no residua are visible in almost 30% of cases, in about 40%, hypodense foci can be depicted, slit-like lesions are present in about 25% of cases, and calcifications can be detected in approximately 10% of cases [14].

Contrast-enhanced CT (CECT) and CT angiography (CTA) can provide additional information in ICH. Several studies could recently demonstrate that an active contrast extravasation on CTA or CECT (referred to as the "spot sign") represents an independent predictor of hematoma growth and predicts mortality [15, 16].

CECT images of acute ICHs have to be investigated carefully in order to depict contrast-enhancing areas in-

Figure 1. 64-year-old male patient with a long-lasting history of arterial hypertension. Unenhanced CT demonstrates a typical hypertensive ICH located in the left thalamus, which is ruptured into the ventricles.

dicative of an underlying neoplasm. As a potential pitfall, subacute and chronic ICH can show a peripheral "ring" enhancement on CECT, which can be present up to 6 months.

Magnetic Resonance Imaging

Within the last years, the value of magnetic resonance imaging (MRI) in the diagnostic work-up of ICH has considerably increased. The MR appearance of ICH on the different sequences changes dramatically depending on time. These changes are due to the typical signal characteristics of the different blood degradation products: oxyhemoglobin, deoxyhemoglobin, methemoglobin, hemosiderin, and ferritin. Up to six different stages of ICHs can be distinguished on MRI performed at field strengths of ≥ 1.0 Tesla [17, 18]: a hyperacute stage (< 6 h), an acute stage (7 h up to 3 days), an early subacute stage (4–7 days), a late subacute stage (1–4 weeks), an early chronic stage (months), and a late chronic stage (months to years) [14, 19–22]. Table 2 summarizes the signal characteristics of the different stages with respect to different MR sequences and indicates the respective blood degradation product, which is responsible for the imaging presentation.

T2*-weighted gradient-echo (T2*w) are exquisitely sensitive to blood residues, and thus are of great value especially in the detection of intracerebral microbleeds [4, 23]. Recently, susceptibility-weighted imaging (SWI) has even been shown to be superior to conventional T2*w in this respect [24, 25].

Interestingly, while a lot of studies on 1.5-Tesla scanners on the MR characteristics of the different stages of ICHs exist, data on the influence of higher field strength (≥ 3 Tesla) are extremely sparse to date [26, 27]. In a pilot study, Allkemper et al. could show that 3-Tesla imaging allows the determination of acute to late subacute ICH stages equivalent to 1.5-Tesla results, but all parts of acute and early subacute ICHs showed significantly increased hypointense signal intensities at 3 Tesla compared to 1.5 Tesla [26]. At field strengths < 1.0 Tesla (0.02–0.5 T), some characteristic features of ICHs such as a central area of hypointensity in acute lesions and a parenchymal rim of hypointensity on late to chronic lesions on T2-weighted (T2w) images cannot be observed [18].

Digital Subtraction Angiography

In the era of CTA and MR angiography (MRA), there are still several indications for the use of digital subtraction angiography (DSA) in ICHs. It still represents the gold standard to evaluate and classify vascular malfor-

Table 2. Signal characteristics of ICH on different MR sequences dependent on the time from onset [14]. ICH: intracerebral hemorrhage; T1w: T1-weighted sequence; T2w: T2-weighted sequence; T2*-GRE: T2*-weighted gradient-echo sequence.

			MR signal intensity		
ICH stage	**Time from onset**	**Hemoglobin state/ blood degradation product**	**T1w**	**T2w**	**T2*-GRE**
Hyperacute	< 6 h	Intracellular oxyhemoglobin	Isointense	Hyperintense (may have hypointense rim)	Hypointense
Acute	7 h–3 days	Intracellular deoxyhemoglobin	Isointense	Hypointense	Profoundly hypointense
Early subacute	4–7 days	Intracellular methemoglobin	Hyperintense	Hypointense	Profoundly hypointense
Late subacute	1–4 weeks	Extracellular methemoglobin	Hyperintense	Hyperintense	Profoundly hypointense
Early chronic	Months	Extracellular methemoglobin + ferritin/hemosiderin wall	Hyperintense	Hyperintense with pronounced low signal rim	Profoundly hypointense
Late chronic	Months to years	Hemosiderin	Isointense	Hypointense	Profoundly hypointense

mations, especially aneurysms, AVMs and dural arteriovenous fistulas (DAVF). DSA should be performed for diagnostic purposes, if no clear cause of ICH could be depicted using the noninvasive imaging modalities, especially in young, normotensive patients. Furthermore, it is necessary for planning therapeutic approaches in patients with AVMs or DAVFs [28–30].

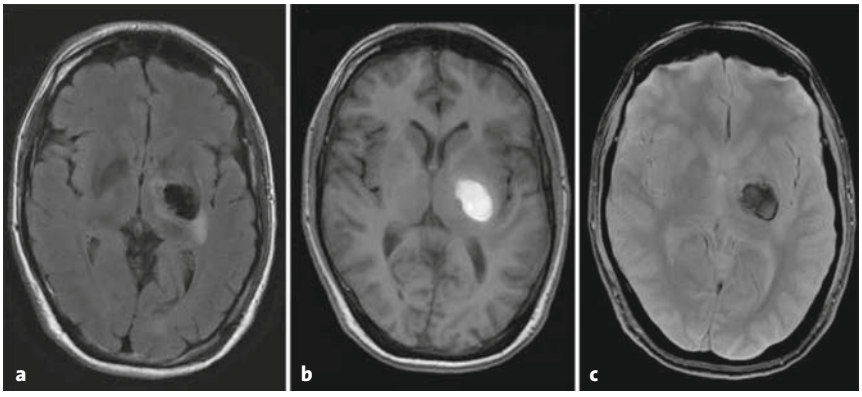

Figures 2a to 2c. Tesla MR images of a 73-year-old female patient with an early subacute hypertensive hemorrhage within the left thalamus, internal capsule, and globus pallidus. MRI was performed 5 days after symptom onset. a) FLAIR images; b) T1-weighted image; c) T2*-weighted image.

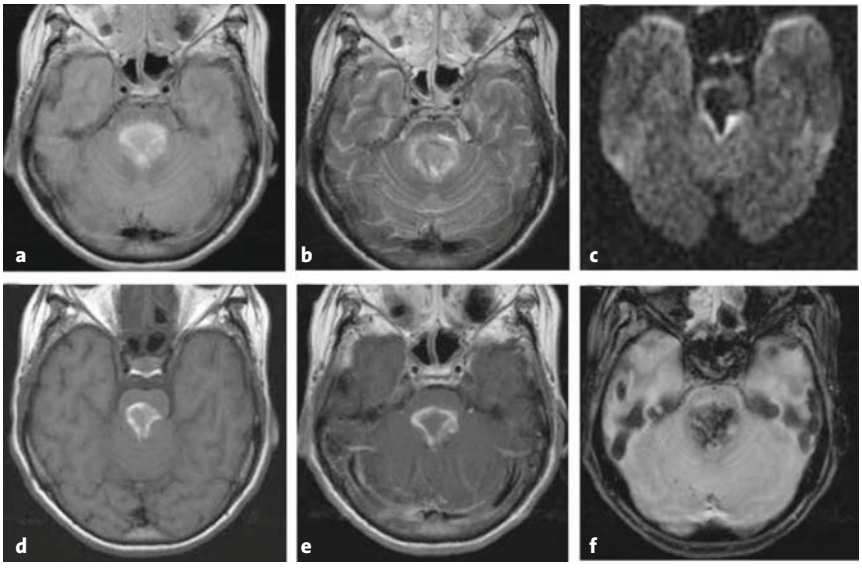

Figures 3a to 3f. 57-year-old female patient with arterial hypertension presenting with sudden onset of severe headache, vomiting, and impaired consciousness. MRI performed 1 week after symptom onset demonstrates a hypertensive ICH located in the pons. a) Proton-density-weighted image; b) T2-weighted image; c) diffusion-weighted image (B-value = 1,000); d) T1-weighted image; e, f) contrast-enhanced T1-weighted axial (e) and coronal (f) images.

Hypertensive Intracerebral Hemorrhage

Arterial hypertension represents the most common cause of nontraumatic ICH in patients between 40 and 70 years of age and accounts for over 50% of cases [22, 23]. Thus, it constitutes by far the most important modifiable risk factor for spontaneous ICH [1, 9, 10, 32]. Elderly males are most commonly affected. Control of hypertension by use of adequate antihypertensive therapy reduces the incidence of ICH [33, 34].

Chronic arterial hypertension results in microangiopathic changes of small penetrating arteries (50–200 µm) originating – most commonly – from the middle cerebral artery, or from the anterior or posterior cerebral arteries, or from the basilar artery. Histomorphologically, severe arteriosclerosis and thickening of the vessel walls due to lipohyalinotic changes (known as lipohyalinosis, plasmatic vascular destruction, or hypertensive fibrinoid necrosis) [35] as well as pseudoaneurysms indicating a degeneration of the media and smooth vessels [36] are observed.

The microvascular changes result in a reduced compliance of the vessel walls, and thus in an impaired vasoreactivity in response to elevations of blood pressure, resulting in vessel wall rupture and hypertensive macro- or microhemorrhages. Different stages of microangiopathic changes can be differentiated microscopically and correlate to the duration and severity grade of the underlying hypertension. In most severe stages, petechial microhemorrhages are regularly observed, with multifocal microbleeds being present in 1–5% of cases [37, 38].

Hypertensive macrohemorrhages are most commonly found in the basal ganglia (60–65%), the thalamus (15–25%), and brain areas, which are supplied by small perforating arteries from the middle and posterior cerebral artery (Figures 1 and 2). The pons and the cerebellum are affected in 10% of cases (Figure 3), while lobar hemorrhages account for 5–15% of cases with hypertensive ICH [39]. Although secondary intraventricular hemorrhages (IVHs) can occur in any

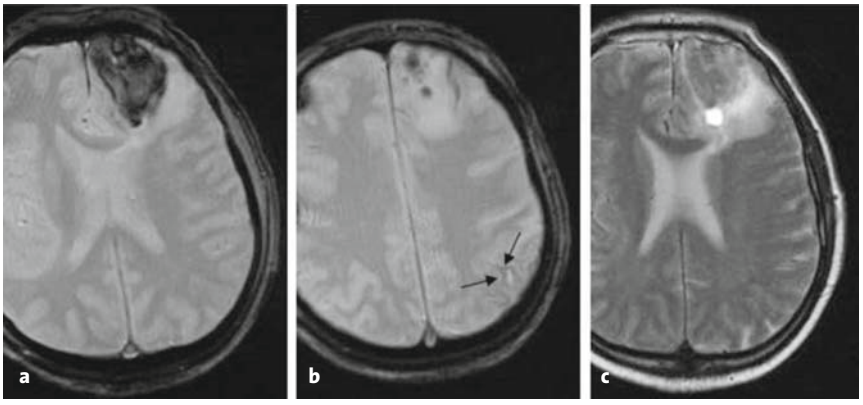

Figures 4a to 4c. 66-year-old male patient with biopsy-proven cerebral amyloid angiopathy. T2*-weighted (a, b) and T2-weighted (c) images reveal an intracerebral macrohemorrhage in the left frontal lobe. Furthermore, the T2*-weighted images depict linear superficial hemosiderosis in the left parietal lobe (b, arrows).

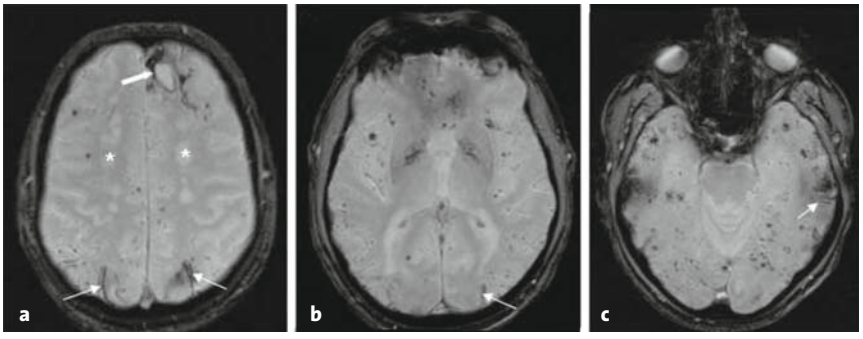

Figures 5a to 5c. 75-year-old male patient with histologically proven cerebral amyloid angiopathy. T2*-weighted images reveal a multitude of small, dot-like microhemorrhages, predominately in a corticosubcortical localization, as well as linear superficial hemosiderosis in both parietal lobes (a, b, thin arrows) and the left temporal lobe (c, thin arrow). A left frontal macrohemorrhage has been evacuated surgically 1 year ago (a, thick arrow).

ICH, thalamic hemorrhages are especially prone to rupture into the ventricles. IVH can result in hydrocephalus due to impairment of cerebral spinal fluid circulation resulting from blood clots within the foramina or the aqueduct, and represents a risk factor for poor outcome [40] (Figure 1).

Imaging Recommendations and Diagnostic Clues

Computed Tomography

A round- to oval-shaped hyperdense parenchymal mass centered within the basal ganglia (putamen and external capsule) and/or the thalamus represents the typical CT appearance of an acute hypertensive ICH (Figure 2). Mixed densities might rarely be observed in cases of active bleeding or a coagulopathy as coincident finding. Additional findings such as parenchymal herniation in cases of large hematomas, and hydrocephalus in cases of secondary IVH might also be present (Figure 1).

Magnetic Resonance Imaging

On MRI, the imaging appearance of the hypertensive hemorrhage depends on its age as detailed above. T2*w images can reveal additional (multifocal) microbleeds predominately in the basal ganglia, thalami and brain stem or cerebellum in long-standing hypertension.

MRA, CTA as well as DSA can show an elongation of the intracranial vessels in patients with severe hypertension, but are otherwise typically normal in hypertensive hemorrhages. Thus, in "typical" cases of an acute basal ganglia or thalamic hemorrhage in an elderly, hypertensive patient, angiographic techniques are not necessary to establish a diagnosis. However, in cases of atypically located hematomas, e.g., lobar or subcortical hemorrhages, CTA or DSA are indicated to exclude secondary causes such as AVM or DAVF. In this respect, it has to been taken into account that DSA still represent the gold standard for the diagnosis of an arteriovenous cerebral malformation [28–30] (see below).

Intracerebral Hemorrhage Related to Cerebral Amyloid Angiopathy

CAA is defined as the deposition of β-amyloid protein in wall of the blood vessels of the cerebral cortex and leptomeninges. Sporadic forms, which are associated with the ε4 allel of the apolipoprotein E and polymorphisms in the presenilin-1 gene, must be differentiated from a variety of hereditary forms, such as the Dutch type [13, 41, 42].

ICH represents the most important clinical presentation of CAA and CAA accounts for 15–20% of all primary ICHs in patients > 60 years, thus it constitutes a major risk factor for ICH in elderly patients [43]. CAA must be considered to be the cause of an ICH if the patient is > 55 years, and MRI reveals a single lobar, cortical, or corticosubcortical hemorrhage without another

cause (Figure 4), multiple hemorrhages, or some hemorrhage in an atypical location [44]. There exist diagnostic criteria for CAA, the so-called Boston criteria, which use clinical data, imaging signs, and, if available, histopathologic findings for the diagnosis of *possible* CAA, *probable* CAA, *probable* CAA *with supporting pathology*, and *definite* CAA [13, 44] (Table 3). An attempt to validate these criteria demonstrated a good correlation between the diagnosis of *probable* CAA according to the criteria and the pathologic diagnosis of CAA, yet the specificity of the diagnosis of *possible* CAA was only 62% [44]. The *definite* diagnosis of CAA according to the Boston diagnostic criteria requires the histopathologic demonstration of vascular amyloid. Thus, a full postmortem examination is still the "gold standard" for the diagnosis of CAA.

Besides lobar macrohemorrhages, microbleeds are a common finding in CAA. Contrary to hypertensive microbleeds, they are typically found in a corticosubcortical localization and predominately within the parietal lobes [45] (Figure 5).

Recently, superficial cortical hemosiderosis – defined as linear blood residues in the superficial layers of the cerebral cortex – has been proposed as a promising MRI criterium for CAA [46, 47] (Figures 4 and 5), but studies on larger patient populations are necessary to determine the value of this sign for the noninvasive diagnosis of CAA.

Besides CAA and hypertensive microangiopathy, common differential diagnoses of cerebral microbleeds on T2*w imaging include multiple cavernomas (Figure 6) and sheer injuries after head trauma.

Table 3. Boston diagnostic criteria for cerebral amyloid angiopathy (CAA) [13, 44].

Definite CAA
Full postmortem examination demonstrating:
- Lobar, cortical, or corticosubcortical hemorrhage
- Severe CAA with vasculopathy
- Absence of other diagnostic lesion

Probable CAA with supporting pathology
Clinical data and pathologic tissue (evacuated hematoma or cortical biopsy) demonstrating:
- Lobar, cortical, or corticosubcortical hemorrhage
- Some degree of CAA in specimen
- Absence of other diagnostic lesion

Probable CAA
Clinical data and MRI or CT demonstrating:
- Multiple hemorrhages restricted to lobar, cortical, or corticosubcortical regions (cerebellar hemorrhage allowed)
- Age $\geq$ 55 years
- Absence of other cause of hemorrhage

Possible CAA
Clinical data and MRI or CT demonstrating:
- Single lobar, cortical, or corticosubcortical hemorrhage
- Age $\geq$ 55 years
- Absence of other cause of hemorrhage

Imaging Recommendations and Diagnostic Clues

Computed Tomography

CT typically depicts a large acute ICH in a lobar, subcortical region, and can show residues af older macrohemorrhages, and a certain amount of leukoencephalopathy.

Magnetic Resonance Imaging

MRI including T2*w images are absolutely recommended if CAA is suspected. This sequence not only demonstrates the acute ICH, but is also very sensitive for all kind of old blood residues: macrohemorrhages, microhemorrhages, as well as superficial siderosis. Besides, a T2w or a fluid-attenuated inversion recovery (FLAIR) sequence should be performed to reveal leukoencephalopathic changes.

Multidetector-row CT angiography (MDCTA), MRA, and DSA are typically normal in patients with CAA.

Cerebral Venous and Sinus Thrombosis

CVSTs account for approximately 1–2% of all strokes in adults [48] and affect all age groups with an estimated annual incidence of 3–4 cases per million in adults [49]. Women represent 75% of all adult cases [50, 51]. The clinical presentation of CVST is highly variable as it depends on a variety of factors such as patient's age [52, 53], the presence of parenchymal involvement, the interval from symptom to diagnosis [54], and the site and the extent of the thrombosis [55, 56]. Common clinical signs include headaches, seizures, focal neurologic deficits, and an impaired level of consciousness [57, 58]. Involvement of the deep veins in cerebral venous occlusive disease has been shown to be a risk factor for death and long-term sequelae [50]. The cortical veins can be rarely affected in an isolated form or – more commonly – in combination with a thrombotic occlusion of the sinuses. There is evidence that the involvement of the cortical veins in sinus thrombosis is of prognostic value.

CVST can result in venous hypertension and parenchymal edema or infarction, as well as in ICH. Early ICH – present at the time of diagnosis of CVST – is observed in approximately 40% of patients with CVST

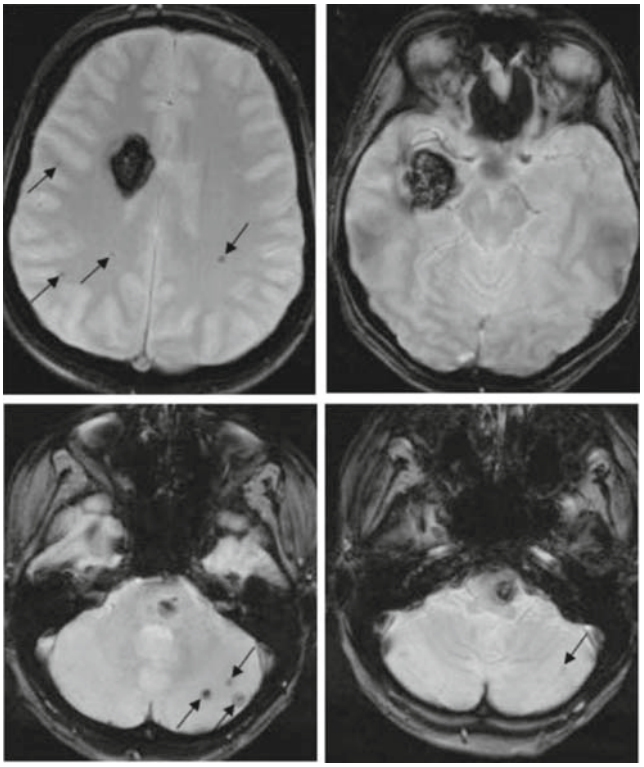

Figure 6. 35-year-old male patient with multiple intracerebral cavernomas. T2*-weighted images depict three large cavernomas and a multitude of further, small cavernomas indicated by the arrows.

[51], and is typically associated with a more severe clinical presentation at onset and a worse outcome [50, 51].

Imaging Recommendations and Diagnostic Clues

Computed Tomography

On CT, direct signs of CVST include the cord sign (or dense vein sign) on unenhanced CT, as well as the empty delta sign on CECT examinations. The cord sign is defined as a homogeneous, increased attenuation of the thrombotic material in the affected vessels [59] and reflects a newly formed thrombus. After 7–14 days the thrombus becomes iso- and then hypodense [59]. The empty delta sign on CECT represents a triangular area of contrast enhancement with a center of relatively low attenuation [60, 61]. It is typically found in the superior sagittal sinus. Indirect signs of CVST include ICH and edema [60] (Figure 7).

Magnetic Resonance Imaging

In the past decade, MRI has replaced DSA in the imaging diagnosis of CVST [62–65], and recent sudies also revealed a comparably high diagnostic value of

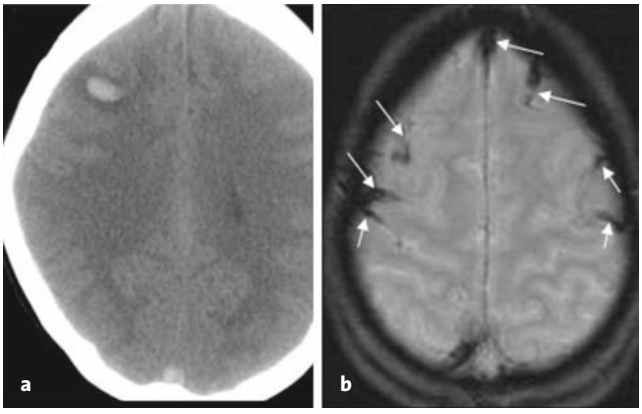

Figures 7a and 7b. 27-year-old female patient with a thrombosis of the superior sagittal sinus and the frontal and parietal cortical veins bilaterally. a) Unenhanced CT shows a small ICH in the right frontal lobe as an indirect sign. b) The T2*-weighted image clearly demonstrates the thrombosed sinus and cortical veins as profoundly hypointense linear structures (arrows).

MDCTA for the diagnosis of sinus thrombosis [66, 67]. Until now, data on the value of this technology for deep or cortical venous thrombosis are currently lacking. On MDCTA, thrombotic material is visualized indirectly by demonstration of contrast filling defects [66]. The following MDCTA parameters can be recommended: 120 kV, 120–140 mAs, collimation = 4 × 1.0 mm, 120 ml contrast agent with an iodine concentration of 300 mg/ml, injection rate of 5 ml/s, and a delay of 35 s [66].

On MRI, the signal characteristics of the thrombotic material within the cerebral veins and sinuses on the different MR sequences are complex and time-dependent [63]. Thus, MRI in CVST has to be interpreted carefully, as there are several potential diagnostic pitfalls [56, 63]. In the first days of an acute CVST, the intravasal clot has a hypointense signal on T2w images and an isointense signal in T1w spin-echo sequences [64]. Thus, these sequences are not very sensitive especially in the acute phase of CVST. After several days the clot becomes hyperintense on T1w images [65, 66].

Venous time-of-flight (TOF) MRA, contrast-enhanced venous MRA, as well as phase-contrast techniques can be used to directly depict the cerebral veins and sinuses [69, 70]. To avoid pitfalls in the interpretation of a venous TOF-MRA, it has to be considered, that a subacute, hyperintense thrombus can potentially simulate flow [56], and that the lack of flow in a vessel might be caused by acute thrombosis, but it might also be due to hypoplasia or aplasia of the respective vessel [56, 63, 72].

Recently, T2*w image sequences have been shown to be of great value in the diagnosis of CVST, and espe-

cially in the diagnosis of cortical venous involvement [65, 68]. They directly visualize the thrombosed veins as profound hypointense tubular structures (Figure 7).

Compared to CT, MRI is more sensitive in the detection of associated parenchymal changes [50]. While FLAIR and proton density (PD)/T2-dual echo sequences provide the best visualization of parenchymal edema, T2*w images show the highest sensitivity for associated hemorrhages and hemorrhagic inhibitions.

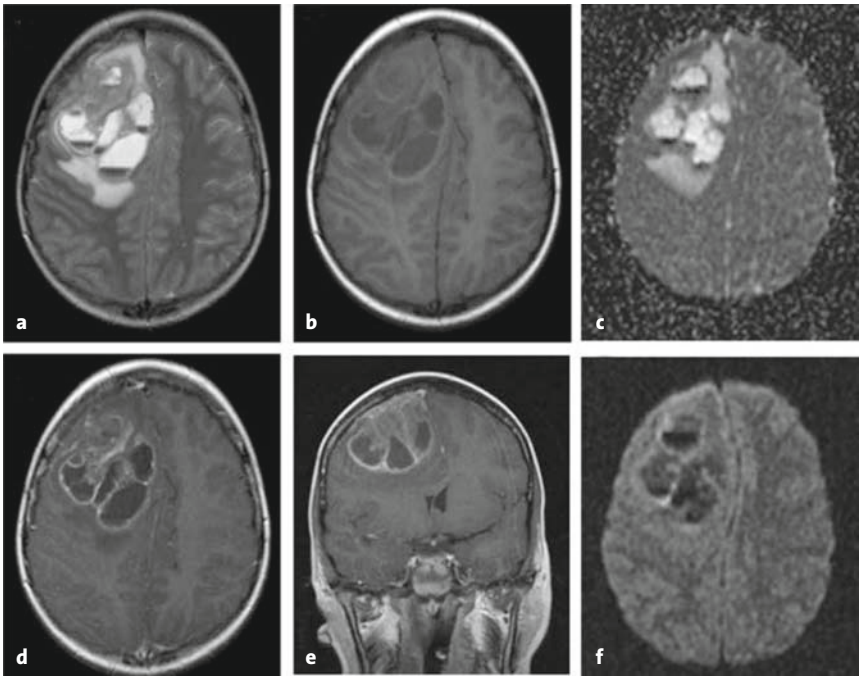

Figures 8a to 8f. 12-year-old child with a large right frontal metastasis of a rhabdomyosarcoma. The cystic areas within the metastasis show several blood-fluid levels. a) T2-weighted image; b) T1-weighted image; c, f) diffusion-weighted images (c, B-value = 50; f, B-value = 1,000); d, e) contrast-enhanced T1-weighted images.

Hemorrhagic Ischemic Stroke

Hemorrhagic ischemic stroke is defined as a secondary hemorrhage within the region of an ischemic cerebral infarction. It can present either as a heterogeneous petechial hemorrhagic transformation or as a secondary parenchymatous hematoma of various extent [73]. Both types of secondary hemorrhages are found in supratentorial territorial infarctions. Fisher & Adams, who observed hemorrhagic transformation in an autopsy study, established the migration theory: the hemorrhagic transformation may be caused by restoration of flow to injured capillaries following embolic obstruction [74]. MRI data confirm this concept: local reperfusion was often accompanied by a persistent perfusion deficit within the remaining perfusion abnormality [75]. Mayer et al. observed hemorrhagic transformation to be as frequent in thrombosis as in embolic stroke [76]. While hemorrhagic transformation has no influence on the neurologic status [76], parenchymal hematoma exceeding one third of the ischemic lesion volume is associated with clinical deterioriation and a poor prognosis [77].

Imaging Recommendations and Diagnostic Clues

With regard to the detection of hemorrhagic transformations in patients with ischemic stroke, MRI including T2*w gradient-echo MR images depicted more hemorrhages and had higher intra- and interobserver agreement compared to CT. Thus, this sequence is strongly recommended for the evaluation of hemorrhagic transformations. It vizualizes the petechial hemorrhages as circumscript hypointense regions within the ischemic area [78].

Intracranial Neoplasms

Primary (malignant) intracerebral tumors as well as parenchymal metastases of extracranial tumors can present with intratumoral hemorrhage, either as first clinical presentation or during the course of the disease. In the literature, the incidence of intratumoral ICH is 1–15% [79, 80]. Hemorrhage is more common in metastatic than in primary brain tumors [81].

In a series of 905 patients with cerebral tumors, 14.6% presented with a macroscopic or microscopic brain hemorrhage on pathologic evaluation [82].

Concerning brain metastases, malignant melanomas, lung cancer, hypernephroma, thyroid cancer, and chorion carcinoma are especially prone to intralesional hemorrhage [83] (Figure 8). With regard to primary intraaxial tumors, intratumoral hemorrhage is most commonly observed in malignant gliomas (glioblastomas, oligodendrogliomas; Figure 9), meningiomas, schwannomas, subependymomas, as well as in primitive neuroectodermal tumors [84–87].

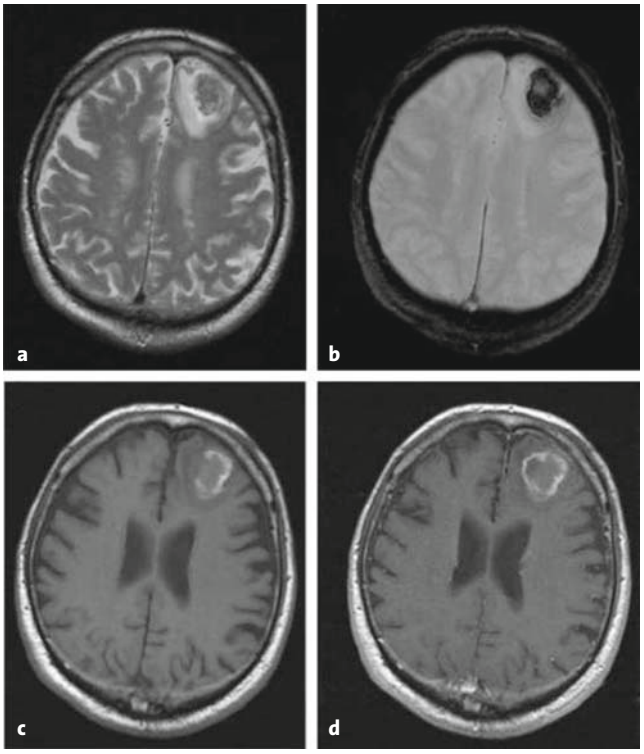

Figures 9a to 9d. 65-year-old female patient with a left frontal ICH. Contrast-enhanced T1-weighted image (d) shows a contrast enhancement of the medial border of the lesion. A neoplasm was suspected and surgery revealed a glioblastoma. a) T2-weighted image, b) T2*-weighted image, c) T1-weighted image.

Possible underlying pathomechanisms of intratumoral hemorrhages include rapid tumor necrosis, invasion of parenchymal blood vessels by the tumor, and rupture of newly formed blood vessels [83]. Clinically, intratumoral hemorrhages typically present with an acute onset of symptoms, such as headache or seizures.

Imaging Recommendations and Diagnostic Clues

In case of metastasis, unenhanced CT or MRI scans typically depict multiple intracerebral lesions, one or several of which show intralesional densities (on CT) or signal intensities (on MRI, respectively) of an ICH.

The presence of a pronounced perilesional edema adjacent to an ICH immediately after the onset of the clinical symptoms is indicative of an intratumoral hemorrhage, caused either by metastasis or by a primary intracerebral tumor. Furthermore, a significant contrast enhancement of the lesion on contrast-enhanced CT or MRI early in the clinical course also strongly suggests an underlying tumor (Figure 9).

Depending on the localization of the tumor, the ICH may be strictly intratumoral (Figure 9) and intraparenchymal or it may rupture into the subdural or subarachnoid space, or into the ventricles.

According to Atlas et al., intratumoral hemorrhages typically show a more heterogeneous signal (Figure 8), decreased or absent hemosiderin within the hemorrhage, and a delayed pattern of hematoma evolution compared to other ICHs [88].

Despite the above-mentioned diagnostic criteria, the identification of a primary or secondary tumor as the underlying cause of an ICH can be very challenging, especially in cases of a large hemorrhage. Thus, the definite exclusion of an underlying tumor requires follow-up scans after resorption of the ICH. Furthermore, it has to been taken into account, that there are no pathognomonic features on contrast-enhanced CT or MRI that definitely distinguish brain metastases from primary malignant brain tumors, therefore a tissue diagnosis by biopsy should always be obtained in patients with unknown primary tumor before therapy [89].

Intracranial Vascular Malformations

Intracranial vascular malformations (IVMs) include AVMs, DAVFs, cavernous malformations (= cavernomas, CMs), and developmental venous anomalies (DVAs). All together, IVMs are the most common cause of primary intracerebral hemorrhage in young adults [90].

ArterioVenous Malformations

Brain AVMs are defined as vascular malformations with arteriovenous shunting in the absence of an intervening capillary bed. Microscopically, the feeding arteries are typically enlarged but mature vessels, the draining veins are also significantly enlarged and can show associated varices or stenoses, as well as aneurysms. In addition to the feeding arteries and the draining vessels, an AVM shows a so-called nidus, namely a conglomeration of numerous small arteriovenous shunts with thin-walled dysplastic vessels.

AVMs equally affect males and females and all ethnic groups. They typically present clinically either with hemorrhage (approximately 50%), seizures (29%) or other focal neurologic deficits (20–25%) at the age of 20–40 years [91].

AVMs widely vary in size from microscopic to giant. According to their size, their location, and their venous

drainage, brain AVMs are surgically classified into three different groups (Spetzler-Martin scale [92]) to estimate the surgical risk.

85% of brain AVMs are found in a supratentorial location, compared to 15% within the posterior fossa. The great majority of AVMs are sporadic forms, while in about 2% of cases, multiple, usually syndromic AVMs are found (craniofacial arteriovenous metameric syndromes, CAMS) [93].

Imaging Recommendations and Diagnostic Clues

Computed Tomography

Unenhanced CT typically fails to reveal an underlying AVM, especially if a large ICH is present. In some cases, enlarged, serpentine vessels and calcifications can be found. MDCTA depicts the enlarged vessels of the AVM, especially the large draining veins. Nevertheless, in case of ICH, small underlying AVMs easily can be missed on both enhanced CT and on MDCTA.

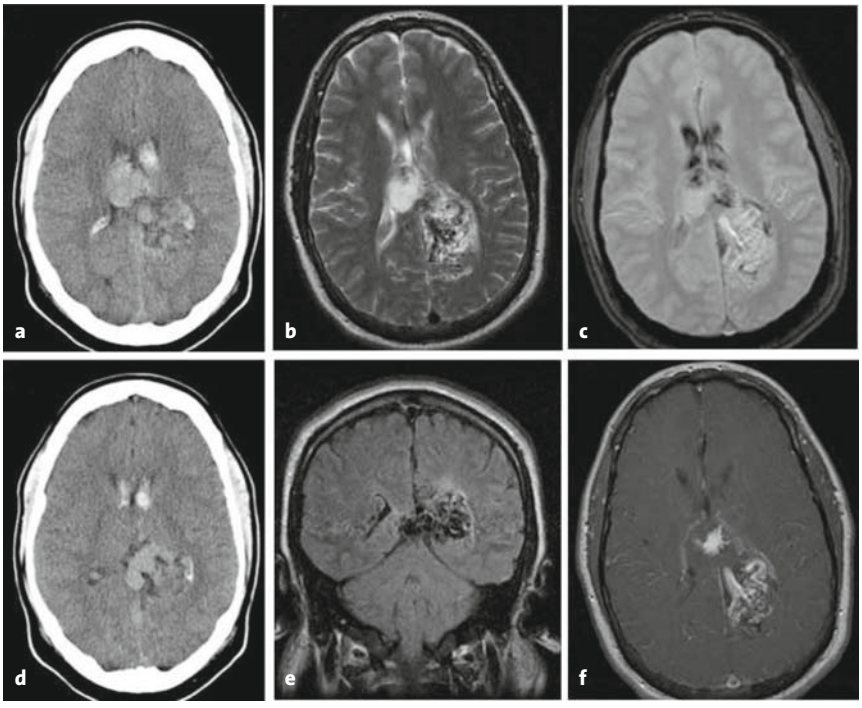

Figures 10a to 10f. 24-year-old male patient with a large arteriovenous malformation (AVM) located within the left precuneus. a, d) Unenhanced CT clearly demonstrates the ICH within the corpus callosum, the precuneus, and the lateral ventricles. The AVM is best depicted as a "bag of black worms" in the b) T2- and e) FLAIR-weighted images. c) T2*-weighted image; f) contrast-enhanced T1-weighted image.

Magnetic Resonance Imaging

On T2w sequences, the AVM vessels are depicted as prominent hypointense flow voids resembling a "bag of black worms" with little or no mass effect (Figure 10), which are best seen on thin (≤ 3 mm) slices. The FLAIR sequence might show a high signal in some of the adjacent brain parenchyma, indicating gliotic tissue. A "traditional" TOF-MRA can allow the gross depiction of the AVM but does not provide sufficient information on the angioarchitecture of the AVM. Recently, high-resolution contrast-enhanced as well as time-resolved MRA techniques have strongly improved the value of MRA in the evaluation of an AVM [28, 94, 95]: Taschner et al., e.g., found a good to excellent intermodality agreement between time-resolved MRA and DSA findings with respect to arterial feeders, nidus size, and venous drainage [95] and Hadizadeh et al. demonstrated a 100% agreement between time-resolved MRA and DSA with regard to the Spetzler-Martin classification [28].

However, there exist no studies on the value of these techniques in the initial detection of a (small) AVM in the acute setting of a (large) ICH. Thus, to definitely exclude an AVM as the source of an ICH, a DSA still is required.

Digital Subtraction Angiography

DSA still remains the gold standard not only for the pretherapeutic evaluation of an AVM but also for the diagnosis of an AVM as the underlying cause of an ICH.

DSA, including selective catheterization of the feeding arteries, delineates the internal architecture of an AVM by clearly depicting the enlarged feeding arteries, the nidus, as well as the early appearance of the shunted enlarged draining veins. A DSA examination should always include selective catheterizations of both internal and external carotid arteries and of the vertebral circulation in order to identify all feeders and in order to examine a potential dural arterial supply of the AVM.

Attention must be drawn to the fact that even DSA might fail to depict a small AVM in case of a large ICH

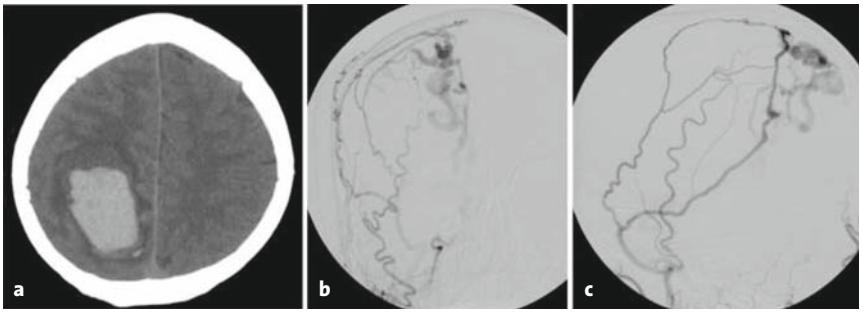

Figures 11a to 11c. a) Unenhanced CT demonstrates a large, right-sided lobar ICH. Digital subtraction angiography reveals a right-sided dural arteriovenous fistula as the underlying pathology. b, c) Selective catheterization of the right external carotid artery.

with a significant mass effect. Therefore, if no bleeding source can be identified and the clinical and imaging presentation of an ICH is not typical of a primary ICH, follow-up imaging including MRI and eventually DSA after the resorption of the hemorrhage is strongly recommended especially in younger patients to exclude an AVM.

Dural ArterioVenous Fistulas

DAVFs are defined as arteriovenous shunts, which are located within the dura mater. They represent approximately 10–15% of all cerebrovascular malformations with AV shunting [96, 97]. The transverse sinus is the most common site of cranial DAVFs, followed by the cavernous sinus. Nevertheless, the shunts can occur anywhere along the dura. Typically, a thrombotic occlusion of the involved dural venous sinus is found [97].

DAVFs in adults are usually acquired and present clinically in middle-aged or elderly patients, preferentially in women. They are observed after head trauma, venous occlusion, or venous hypertension, but may also be idiopathic. Most common symptoms include pulsatile tinnitus (in case of affection of the transverse or sigmoid sinus), and pulsatile exophthalmus (in case of cavernous sinus fistulas). In rare cases, DAVFs can present with encephalopathic symptoms, as progressive dementia and parkinsonism due to venous congestion [98]. The risk of ICH from cranial DAVFs primarily depends on their venous drainage pattern, which is reflected in the Cognard classification [75, 97]. A flow reversal in the dural sinus or the cortical veins is associated with an increased risk of hemorrhage [97, 99]. ICH caused by DAVFs is often found in an "atypical", lobar localization (Figure 11).

Imaging Recommendations and Diagnostic Clues

Computed Tomography

Unenhanced CT typically only depicts the ICH and is otherwise normal. Furthermore, also contrast-enhanced CT and MDCTA often fail to reveal the underlying DAVF, but might visualize the thrombotic material within the affected dural sinus. In case of aggressive DAVFs, MDCTA can demonstrate tortuous dural feeders and enlarged cortical drainage vessels.

Magnetic Resonance Imaging

Conventional T2, T1, and FLAIR sequences demonstrate the thrombosed dural sinus and eventually an adjacent edema, if a venous congestion is present. In rare cases, a diffuse dural enhancement is observed on contrast-enhanced T1w images. Arterial TDF-MRA often is negative with regard to the presentation of the shunt, especially in small or slow-flow shunts, while venous TOF-MRA might demonstrate the occluded parent sinus and – eventually – some collateral flow.

In summary, these techniques are not sufficient to exclude a DAVF. Recently, the potential of contrast-enhanced, time-resolved MRA techniques has been assessed by inital studies, which yielded promising results. In their study on 14 DAVFs, Meckel et al. found this technique reliable for the detection of the fistulas, suitable for follow-up, and – within limitations – suitable to classify the DAVFs [100]. Nevertheless, further studies are needed to definitely assess the value of time-resolved MRA.

Digital Subtraction Angiography

Despite the recent advances in noninvasive imaging (MDCTA, time-resolved MRA, CEMRA) DSA still represents the gold standard for the diagnosis of a DAVF. As in case of an AVM, it should always include selective catheterization of both internal and external carotid arteries, and the vertebral arteries. Typically, multiple arterial feeders from dural branches of the external carotid artery are found, followed by feeders from tentorial or dural branches from the internal carotid artery or the vertebral arteries (Figure 11).

Cavernous Malformations and Developmental Venous Anomalies

CMs or cavernomas are defined as benign vascular hamartomas containing a mass of closely apposed dilated immature blood vessels with a single layer of endothelium and no neuronal tissue in between. These thin-walled vessels within the cavernoma resemble sinusoidal cavities filled with stagnant blood. On gross pathologic examination they appear as a "mulberry-like" nodule (Figure 12).

The prevalence of sporadic cavernomas in the general population is approximately 0.5% [101]. In up to 25% of the patients, multiple cavernomas are found (Figure 6). Familial (multiple) CM syndrome is an autosomal dominant heriditary disorder with variable penetrance and is typically found in Hispanic Americans [102].

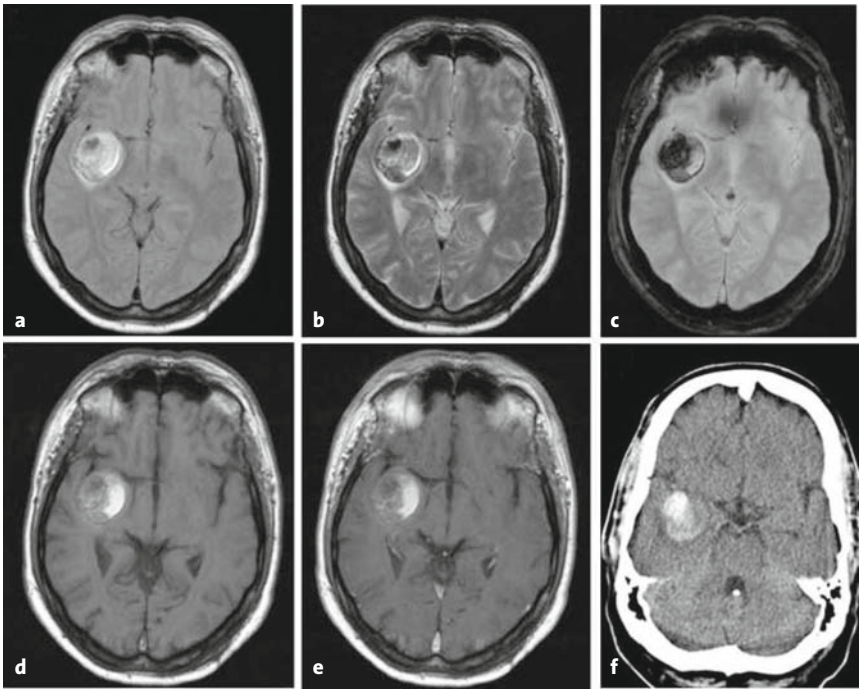

Figures 12a to 12f. 50-year-old male patient with a large, singular cavernoma within the right temporal lobe. a) Proton-density weighted image; b) T2-weighted image; c) T2*-weighted image; d, e) unenhanced (d) and contrast-enhanced (e) T1-weighted images; f) unenhanced CT.

In about 10–20% of patients, cavernomas are asymptomatic and are incidentially diagnosed on cerebral MRI; 30–50% of patients clinically present with seizures, and approximately 20–25% of patients suffer from an ICH. The peak of clinical presentation of sporadic cavernomas is between 30 and 50 years of age. The median age at the time of presentation with an initial ICH is 35 years [103]. Females more often present with ICH than males [103]. Familial forms typically become symptomatic earlier in life.

An initial bleeding risk of 0.3–0.7% per year with rebleeding rates of approximately 5% per year are reported for sporadic forms [104, 105]. Recent studies indicate that the use of higher field strengths and SWI allow the detection of CMs with an even higher sensitivity than conventional gradient-echo MRI [101]. Thus, the bleeding risk per lesion might have been overestimated in older studies.

ICHs due to CMs typically occur at a younger age compared to AVM and DAVF and they tend to be less disabling at onset than those due to AVM and DAVF. This is most probably due to the fact that ICHs caused by CMs are typically smaller than those due to other IVMs [103–105]

CMs can be associated with a DVA [106] (Figure 13). DVAs are defined as congenital IVMs, due to early arrest of medullary veins during embryologic developmental, resulting in persistence of large embryonic deep white matter veins. They present as "Medusa's head" of small stellate veins, converging into a large collector vein, which typically drains into an ependymal vein or a dural sinus. DVAs drain functional brain parenchyma, and thus can be considered anatomic variants of otherwise normal venous drainage [107]. Therefore, care has to be taken, not to touch the DVA in cases of surgical interventions, as this would result in venous infarction. This is especially important in surgical resections of eventually associated CMs. DVAs are usually asymptomatic, unless associated with other malformations as cortical dysplasias are CMs. The risk of hemorrhage in case of a DVA not associated with a CM is extremely low, it increases in case of a thrombosis of the draining vein.

It has to be mentioned that the association between CMs and DVAs is sometimes controversially discussed. In fact, in its original MR description of CMs, Rigamonti et al. [108] included the imaging differential diag-

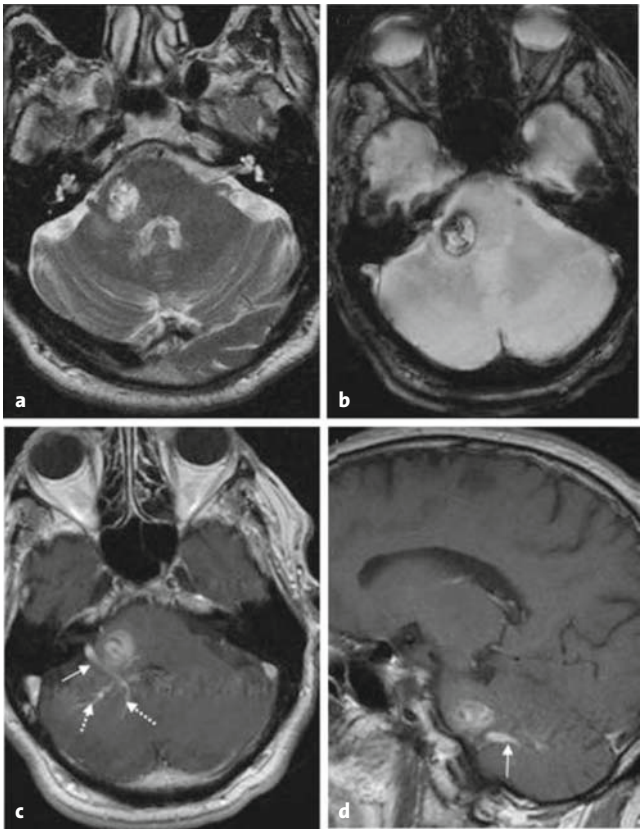

Figures 13a to 13d. 56-year-old female patient with a right-sided cavernoma within the pons and the right middle cerebellar peduncle. Please note that only the contrast-enhanced T1-weighted images reveal the associated developmental venous anomaly (c, d, arrows). a) T2-weighted image, b) T2*-weighted image.

nosis of blood residues as being indistinguishable from CMs. Thus, the exact nature of the cavernoma-like hemosiderin deposit adjacent to CMs is sometimes questionable in cases which have not been pathologically confirmed [109].

Imaging Recommendations and Diagnostic Clues

Computed Tomography

Unenhanced CT can be negative in up to 50% of cases of CM or it can depict the cavernoma as a round, well-delineated hyperdense lesion (Figure 12). These lesions measure typically < 3 cm in diameter and show calcifications in 40–60% of cases. In asymptomatic CMs, no surrounding edema is present. On CECT, the CMs typically show little or no contrast enhancement.

DVAs can typically not be depicted on unenhanced CT, while they are easily visualized on contrast-enhanced CT or MDCTA [110, 111].

Magnetic Resonance Imaging

MRI including a T2*w gradient-echo sequence represents the gold standard for the diagnosis of a CM.

The intralesional signal characteristics of CMs depend on the following variables: presence of different blood degradation products, flow within the caverns, calcifications within the cavernoma, and partially thrombosed areas. Typically, CMs show a hyperintense signal within their center on both T1w and T2w sequences, and a hypointense rim, due to hemosiderin deposits. Nevertheless, the center can also show mixed signal intensities (Figures 6, 12, and 13).

Top differential diagnosis of CMs include: thrombosed aneurysm, old primary ICH, and intratumoral ICH [108].

Coagulopathies and Drug-Related Intracerebral Hemorrhage

A wide variety of systemic causes of coagulopathias can result in ICH.

Congenital Bleeding Disorders

Hemophilia represents the congenital bleeding disorder with the highest prevalence [112]. In hemophilic patients, ICH is of significant importance for morbidity and mortality [113]. In addition to hemophilia, other rare congenital disorders can present with ICH. Those include von Willebrand factor deficiency, congenital afibrinogenemia, and deficiencies in certain coagulation factors V, VII, XIII, or X. Even less frequently, genetically hypercoagulable states such as antiphospholipid syndrome, prothrombin mutation, and factor V Leyden deficiency can result in secondary ICH due to CVST [112].

Coagulopathic Liver Disease

Hepatic dysfunction is a common cause of thrombocytopenia and coagulopathy. However, the role of coagulopathic liver disease in spontaneous ICH is discussed controversialy. While some authors found a significant correlation [114, 115], Lee & Hinrichs observed no case of spontaneous ICH in a prospective series of 100 patients with severe liver disease and coagulopathy [116].

Neoplastic Coagulopathies Causing Intracerebral Hemorrhage

Coagulopathies are a major cause of ICH in cancer patients and they are most often seen in patients with leukemia, especially in AML [81, 117] (Figure 14). Acute dis-

seminated intravascular coagulation (DIC) is the typical underlying pathomechanism in neoplastic coagulopathies. Hemorrhages can affect the brain parenchyma, the ventricles, or the subdural or subarachnoid spaces. Graus et al. reported the prevalence of neoplastic coagulopathy in 14.6% of patients with systemic cancer [117]. Clinical signs of hemorrhage may be acute or gradual and include headache, vomiting, and encephalopathy. Especially in leukemia, the clinical signs of ICH are often fulminant and may be fatal [81]. Cranial imaging in acute DIC usually reveals a single ICH located in the white matter.

Thrombocytopenia

Any condition that results in a low platelet count predisposes a patient to bleeding disorders, including ICH. Thrombocytopenia has multiple causes, and can be due to either decreased platelet production (observed in certain congenital disorders and cases of bone marrow damage due to radiation or drugs) or to increased platelet destruction, as, e.g., in idiopathic thrombocytopenic purpura. Severe thrombocytopenia usually causes multiple hemorrhages.

Drug-Induced Intracerebral Hemorrhage

Antimalarial agents, antiepileptic medications, furosemide, digoxin, and estrogens are known to induce thrombocytopenia, which can result in ICH [112]. Furthermore, different chemotherapeutic agents such as L-asparaginase, used in the induction chemotherapy of acute lymphocytic leukemia, can cause ICH [118].

Excessive use of alcohol also increases the risk of ICH by impairing coagulation and directly affecting the integrity of cerebral vessels [119].

Anticoagulants and thrombolytic agents increase the risk of ICH. The risk of ICH under therapy with warfarin is approximately 0.5–1% per year, while on the other hand, 5% of all ICHs occur in patients under warfarin or heparin [112]. Furthermore, anticoagulants increase the risk of secondary hemorrhagic transformation or imbibition of patients with ischemic strokes.

After thrombolytic therapy in patients with myocardial infarctions, the risk of ICH is 0.5–2%, while it is 6–15% in patients with thrombolytic therapy of ischemic stroke [120] (Figure 15).

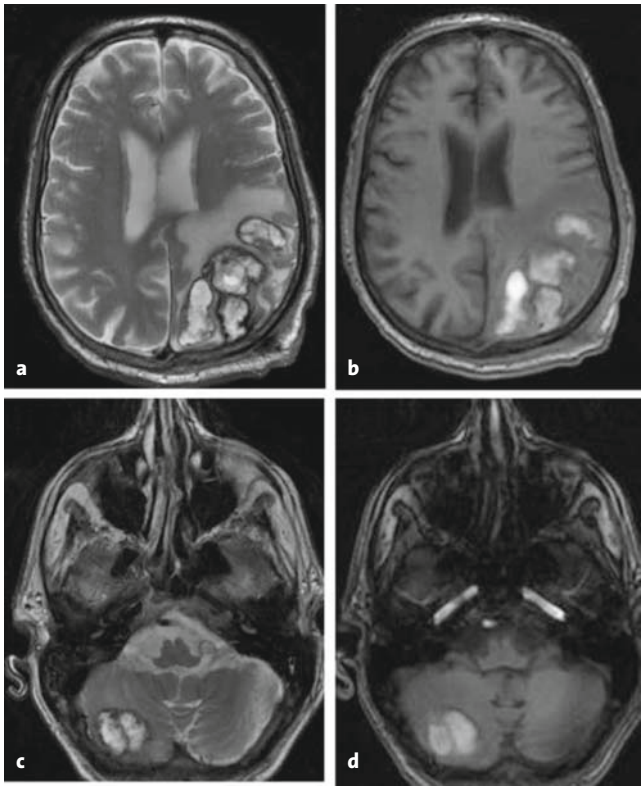

Figures 14a to 14d. 35-year-old patient with acute myelid leukemia and associated coagulopathy. MRI reveals multiple ICHs within the left parietal and occipital lobes (a, b), as well as in the right cerebellar hemisphere (b, c). a, c) T2-weighted images; b, d) T1-weighted images.

ICHs are typically rather large in these patients, are located within the subcortical white matter, often show fluid levels, and inhomogeneous signal intensities due to different stages of blood degradation products [112, 121] (Figure 15). The ICHs related to thrombolysis are typically lobar (70–90%) and multiple (30%) [122, 123].

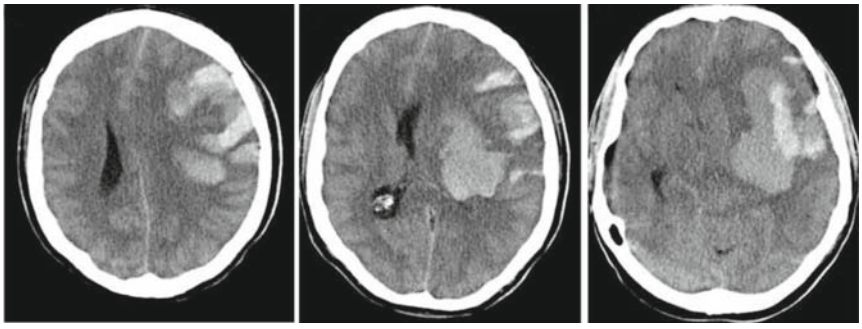

Figure 15. 67-year-old male patient 12 h after thrombolytic therapy of an acute ischemic stroke. CT images reveal a large hemorrhage in the territory of the left middle cerebral artery. As is typical of ICH after thrombolytic therapy, inhomogeneous signal densities due to different stages of blood degradation products are present.

Conclusion

In summary, ICH can reflect a wide variety of primary and secondary causes. Noninvasive diagnosis of underlying pathologies has improved dramatically with the advances in MDCTA and MR imaging, such as SWI and time-resolved MRA. Nevertheless, to date, conventional DSA still remains the gold standard for the detection and pretherapeutic evaluation of cerebral vascular malformations with arteriovenous shunts.

Conflict of Interest Statement

The authors declare that there is no actual or potential conflict of interest in relation to this article.

References

1. Fewel ME, Thompson BG Jr, Hoff JT. Spontaneous intracerebral hemorrhage: a review. Neurosurg Focus 2003;15:1–16.
2. Qureshi AI, Tuhrim S, Broderick JP, Batjer HH, Hondo H, Hanley DF. Spontaneous intracerebral hemorrhage. NEJM N Engl J Med 2001;344: 1450–60.
3. Foulkes MA, Wolf PA, Price TR, Mohr JP, Hier DB. The Stroke Data Bank: design, methods, and baseline characteristics. Stroke 1988;19:547–54.
4. Chan S, Kartha K, Yoon SS, Desmond DW, Hilal SL. Multifocal hypointense cerebral lesions on gradient-echo MR are associated with chronic hypertension. AJNR Am J Neuroradiol 1996;17:1821–7.
5. Cordonnier C, Al-Shahi Salman R, Wardlaw J. Spontaneous brain microbleeds: systematic review, subgroup analyses and standards for study design and reporting. Brain 2007;130:1988–2003.
6. Koennecke HC. Cerebral microbleeds on MRI: prevalence, associations, and potential clinical implications. Neurology 2006;66:165–71.
7. Caplan LR. General symptoms and signs. In: Kase CS, Caplan LR, eds. Intracerebral hemorrhage. Boston: Butterworth-Heinemann, 1994:31–43.
8. Juvela S, Hillbom M. Palomaki H. Risk factors for spontaneous intracerebral hemorrhage. Stroke 1995;26:1558–64.
9. Thrift AG, McNeil JJ, Forbes A, Donnan GA. Risk factors for cerebral hemorrhage in the era of well-controlled hypertension. Melbourne Risk Factor Study (MERFS) Group. Stroke 1996;27:2020–5.
10. Broderick JP, Brott T, Tomsick T, Miller R, Huster G. Intracerebral hemorrhage more than twice as common as subarachnoid hemorrhage. J Neurosurg 1993;78:188–91.
11. Hart RG, Boop BS, Anderson DC. Oral anticoagulants and intracranial hemorrhage. Facts and hypotheses. Stroke 1995;26:1471–7.
12. Juvela S. Prevalence of risk factors in spontaneous intracerebral hemorrhage and aneurysmal subarachnoid hemorrhage. Arch Neurol 1996; 53:734–40.
13. Greenberg SM, Briggs ME, Hyman BT, Kokoris GJ, Takis C, Kanter DS, Kase CS, Pessin MS. Apolipoprotein E epsilon 4 is associated with the presence and earlier onset of hemorrhage in cerebral amyloid angiopathy. Stroke 1996;27:1333–7.
14. Parizel PM, Makkat S, van Miert E, van Goethem JW, van den Hauwe L, de Schepper AM. Intracranial hemorrhage: principles of CT and MRI interpretation. Eur Radiol 2001;11:1770–83.
15. Kim J, Smith A, Hemphill JC 3rd, Smith WS, Lu Y, Dillon WP, Wintermark M. Contrast extravasation on CT predicts mortality in primary intracerebral hemorrhage. AJNR Am J Neuroradiol 2008;29:520–5.
16. Wada R, Aviv RI, Fox AJ. CT angiography "spot sign" predicts hematoma expansion in acute intracerebral hemorrhage. Stroke 2007;38: 1257–62.
17. Gomori JM, Grossman RI, Goldberg HI, Zimmerman RA, Bilaniuk LT. Intracranial hematomas: imaging by high-field MR. Radiology 1985; 157:87–93.
18. Seidenwurm D, Meng TK, Kowalski H, Weinreb JC, Kricheff II. Intracranial hemorrhagic lesions: evaluation with spinecho and gradient-refocused MR imaging at 0.5 and 1.5 T. Radiology 1989;172:189–94.
19. Bradley WG Jr. MR appearance of hemorrhage in the brain. Radiology 1993;189:15–26.
20. Thulborn KR, Brady TJ. Iron in magnetic resonance imaging of cerebral hemorrhage. Magn Reson Q 1989;5:23–38.
21. Hayman LA, Taber KH, Ford JJ, Bryan RN. Mechanisms of MR signal alteration by acute intracerebral blood: old concepts and new theories. AJNR Am J Neuroradiol 1991;12:899–907.
22. Gomori JM, Grossman RI, Hackney DB, Goldberg HI, Zimmerman RA, Bilaniuk LT. Variable appearances of subacute intracranial hematomas on high-field spin-echo MR. AJR Am J Roentgenol 1988;150:171–8.
23. Viswanathan A, Chabriat H. Cerebral microhemorrhage. Stroke 2006; 37:550–5.
24. Vernooij MW, Ikram MA, Wielopolski PA, Krestin GP, Breteler MM, van der Lugt A. Cerebral microbleeds: accelerated 3D T2*-weighted GRE MR imaging versus conventional 2D T2*-weighted GRE MR imaging for detection. Radiology 2008;248:272–7.
25. Hermier M, Nighoghossian N. Contribution of susceptibility-weighted imaging to acute stroke assessment. Stroke 2004;35:1989–94.
26. Allkemper T, Tombach B, Schwindt W, Kugel H, Schilling M, Debus O, Möllmann F, Heindel W. Acute and subacute intracerebral hemorrhages: comparison of MR imaging at 1.5 and 3.0 T-initial experience. Radiology 2004;232:874–81.
27. Sohn CH, Baik SK, Lee HJ, Lee SM, Kim IM, Yim MB, Hwang JS, Lauzon ML, Sevick RJ. MR imaging of hyperacute subarachnoid and intraventricular hemorrhage at 3T: a preliminary report of gradient echo T2*-weighted sequences. AJNR Am J Neuroradiol 2005;26:662–5.
28. Hadizadeh DR, Falkenhausen M von, Gieske J, Meyer B, Urbach H, Hoogeveen R, Schild HH, Willinek WA. Cerebral arteriovenous malformation: Spetzler-Martin classification at subsecond-temporal-resolution four-dimensional MR angiography compared with that at DSA. Radiology 2008;246:205–13.
29. Fasulakis S, Andronikou S. Comparison of MR angiography and conventional angiography in the investigation of intracranial arteriovenous malformations and aneurysms in children. Pediatr Radiol 2003;33:378–84.
30. Wintermark M, Dillon WP. Advanced CT and MR imaging techniques: an academic whim or a clinical standard in the making? AJNR Am J Neuroradiol 2006;27:1257.
31. Rosenow F, Hojer C, Meyer-Lohmann C, Hilgers RD, Mühlhofer H, Kleindienst A, Owega A, Köning W, Heiss WD. Spontaneous intracerebral hemorrhage. Prognostic factors in 896 cases. Acta Neurol Scand 1997; 96:174–82.
32. Brott T, Thalinger K, Hertzberg V. Hypertension as a risk factor for spontaneous intracerebral hemorrhage. Stroke 1986;17:1078–83.
33. Hypertension Detection and Follow-up Program Cooperative Group. Five-year findings of the Hypertension Detection and Follow-up Program. III. Reduction in stroke incidence among persons with high blood pressure. JAMA 1982;247:633–8.
34. SHEP Cooperative Research Group. Prevention of stroke by antihypertensive drug treatment in older persons with isolated systolic hypertension: final results of the Systolic Hypertension in the Elderly Program (SHEP). JAMA 1991;265:3255–64.
35. Fisher CM. Hypertensive cerebral hemorrhage. Demonstration of the source of bleeding. J Neuropathol Exp Neurol 2003;62:104–47.
36. Cole FM, Yates PO. Pseudo-aneurysms in relationship to massive cerebral hemorrhage. J Neurol Neurosurg Psychiatry 1967;30:61–6.
37. Lee SH, Bae HJ, Ko SB, Kim H, Yoon BW, Roh JK. Comparative analysis of the spatial distribution and severity of cerebral microbleeds and old lacunes. J Neurol Neurosurg Psychiatry 2004;75:423–7.
38. Imaizumi T, Horita Y, Chiba M, Hashimoto Y, Honma T, Niwa J. Dot-like hemosiderin spots on gradient echo T2*-weighted magnetic resonance imaging are associated with past history of small vessel disease in patients with intracerebral hemorrhage. J Neuroimaging 2004;14: 251–7.

39. Cooper JA. Hypertensive intracerebral hemorrhage. In: Osborn AG, ed. Diagnostic imaging: brain. Salt Lake City: Amirsys, 2004:I.4.16–I.4.19.
40. Naff NJ. Intraventricular hemorrhage in adults. Curr Treat Options Neurol 1999;1:173–8.
41. Natté R, Vinters HV, Maat-Schieman ML, Bornebroek M, Haan J, Roos RA, van Duinen SG. Microvasculopathy is associated with the number of cerebrovascular lesions in hereditary cerebral hemorrhage with amyloidosis, Dutch type. Stroke 1998;29:1588–94.
42. Zhang-Nunes SX, Maat-Schieman ML, van Duinen SG, Roos RA, Frosch MP, Greenberg SM. The cerebral beta-amyloid angiopathies: hereditary and sporadic. Brain Pathol 2006;16:30–9.
43. Vinters HV. Cerebral amyloid angiopathy. A critical review. Stroke 1987; 18:311–24.
44. Knudsen KA, Rosand J, Karluk D, Greenberg SM. Clinical diagnosis of cerebral amyloid angiopathy: validation of the Boston criteria. Neurology 2001;56:537–9.
45. Lee SH, Kim SM, Kim N, Yoon BW, Roh JK. Cortico-subcortical distribution of microbleeds is different between hypertension and cerebral amyloid angiopathy. J Neurol Sci 2007;258:111–4.
46. Linn J, Herms J, Dichgans M, Brückmann H, Fesl G, Freilinger T, Wiesmann M. Subarachnoid hemosiderosis and superficial cortical hemosiderosis in cerebral amyloid angiopathy. AJNR Am J Neuroradiol 2008; 29:184–6.
47. Feldman HH, Maia LF, Mackenzie IRA, Forster BB, Martzke J, Woolfenden A. Superficial siderosis: a potential diagnostic marker of cerebral amyloid angiopathy in Alzheimer disease. Stroke 2008;39:2894–7.
48. Bogousslavasky J, Pierre P. Ischemic stroke in patients under age 45. Neurol Clin 1992;10:113–24.
49. Stam J. Current concepts: thrombosis of the cerebral veins and sinuses. N Engl J Med 2005;352:1791–8.
50. Ferro JM, Canhao P, Stam J, Bousser MG, Barinagarrementeria F, ISCVT Investigators. Prognosis of cerebral vein and dural sinus thrombosis: results of the International Study on Cerebral Vein and Dural Sinus Thrombosis (ISCVT). Stroke 2004;35:664–70.
51. Girot M, Ferro JM, Canh OP, Stam J, Bousser MG, Barinagarrementeria F, Leys D, ISCVT Investigators. Predictors of outcome in patients with cerebral venous thrombosis and intracerebral hemorrhage. Stroke 2007;38:337–42.
52. deVeber G, Andrew M, Adams C, Bjornson B, Booth F, Buckley DJ, Camfield CS, David M, Humphreys P, Langevin P, MacDonald EA, Gillett J, Meaney B, Shevell M, Sinclair DB, Yager J, Canadian Pediatric Ischemic Stroke Study Group. Cerebral sinovenous thrombosis in children. N Engl J Med 2001;345:417–23.
53. Ferro JM, Canhão P, Bousser MG, Stam J, Barinagarrementeria F, ISCVT Investigators. Cerebral vein and dural sinus thrombosis in elderly patients. Stroke 2005;36:1927–32.
54. Ferro JM, Lopes MG, Rosas MJ Fontes J, VENOPORT Investigators. Delay in hospital admission of patients with cerebral vein and dural sinus thrombosis, Cerebrovasc Dis 2005;19:152–6.
55. Ferro JM, Canhão P. Acute treatment of cerebral venous and dural sinus thrombosis. Curr Treat Options Neurol 2008;10:126–37.
56. Lafitte F, Boukobza M, Guichard JP, Hoeffel C, Reizine D, Ille O, Woimant F, Merland JJ. MRI and MRA for diagnosis and follow-up of cerebral venous thrombosis (CVT). Clin Radiol 1997;52:672–9.
57. Ameri A, Bousser MG. Cerebral venous thrombosis. Neurol Clin 1992;10: 87–111.
58. Villringer A, Mehraen S, Einhäupl KM. Pathophysiological aspects of cerebral sinus venous thrombosis. J Neuroradiol 1994;21:72–80.
59. Vijay RKP. The cord sign. Radiology 2006;240:299–300.
60. Virapongse C, Cazenave C, Quisling R, Sarwar M, Hunter S. The empty delta sign: frequency and significance in 76 cases of dural sinus thrombosis. Radiology 1987;162:779–85.
61. Lee EJ. The empty delta sign. Radiology 2002;224:788–9.
62. Bianchi D, Maeder P, Bogousslavsky J, Schnyder P, Meuli RA. Diagnosis of cerebral venous thrombosis with routine magnetic resonance: an update. Eur Neurol 1998;40:179–90.
63. Teasdale E. Cerebral venous thrombosis: making the most of imaging. J R Soc Med 2000;93:234–7.
64. Connor SE, Jarosz JM. Magnetic resonance imaging of cerebral venous sinus thrombosis. Clin Radiol 2002;57:449–61.
65. Selim M, Fink J, Linfante I, Kumar S, Schlaug G, Caplan LR. Diagnosis of cerebral venous thrombosis with echo-planar T2*-weighted magnetic resonance imaging. Arch Neurol 2002;59:1021–6.
66. Linn J, Ertl-Wagner B, Seelos KC, Strupp M, Reiser M, Brückmann H, Brüning R. Diagnostic value of multidetector-row CT angiography in the evaluation of thrombosis of the cerebral venous sinuses. AJNR Am J Neuroradiol 2007;28:946–52.
67. Gaikwad AB, Mudalgi BA, Patankar KB, Patil JK, Ghongade DV. Diagnostic role of 64-slice multidetector row CT scan and CT venogram in cases of cerebral venous thrombosis. Emerg Radiol 2008;15:325–33.
68. Idbaih A, Boubokza M, Crassard I, Porcher R, Bousser MG, Chabriat H. MRI of clot in cerebral venous thrombosis. High diagnostic value of susceptibility-weighted images. Stroke 2006;37:991–5.
69. Anzalone N. Contrast-enhanced MRA of intracranial vessels. Eur Radiol 2005;15:Suppl 5:E3–10.
70. Meckel S, Glücker TM, Kretschmar M, Scheffler K, Radü EW, Wetzel SG. Display of dural sinuses with time-resolved, contrast-enhanced three-dimensional MR venography. Cerebrovasc Dis 2008;25:217–24.
71. Renowden S. Cerebral venous sinus thrombosis. Eur Radiol 2004;14: 215–26.
72. Ayanzen RH, Bird CR, Keller PJ, McCully FJ, Theobald MR, Heiserman JE. Cerebral MR venography: normal anatomy and potential diagnostic pitfalls. AJNR Am J Neuroradiol 2000;21:74–8.
73. Hart RG, Easton JD. Hemorrhagic infarcts. Stroke 1986;17:586–9.
74. Fisher CM, Adams RD. Observations on brain embolism with special reference to the mechanism of hemorrhagic infarction. J Neuropathol Exp 1951;10:92–4.
75. Fiehler J, Remmele C, Kucinski TH, Rosenkranz M, Thomalla G, Weiller C, Zeumer H, Röther J. Reperfusion after severe local perfusion deficit precedes hemorrhagic tranbsformation. An MRI study in acute stroke patients. Cerebrovasc Dis 2005;19:117–24.
76. Mayer TE, Schulte-Altedorneburg G, Droste DW, Brückmann H. Serial CT and MRI of ischemic cerebral infarcts: frequency and clinical impact of hemorrhagic transformation. Neuroradiology 2000;42:233–9.
77. Berger C, Fiorelli M, Steiner T, Schabitz WR, Bozzao L, Bluhmki E, Hacke W, Kummer R von. Hemorrhagic transformation of ischemic brain tissue: asymptomatic or symptomatic? Stroke 2001;32:1330–5.
78. Arnould MC, Grandin CB, Peeters A, Cosnard G, Duprez TP. Comparison of CT and three MR sequences for detecting and categorizing early (48 hours) hemorrhagic transformation in hyperacute ischemic stroke. AJNR Am J Neuroradiol 2004;25:939–44.
79. Leeds NE, Sawaya R, van Tassel P, Hayman LA. Intracranial hemorrhage in the oncologic patient. Neuroimaging Clin N Am 1992;2:119–36.
80. Destian S, Sze G, Krol G, Zimmerman RD, Deck MD. MR imaging of hemorrhagic intracranial neoplasms. AJR Am J Roentgenol 1989;152: 137–44.
81. Rogers LR. Cerebrovascular complications in cancer patients. Neurol Clin 2003;21:167–92.
82. Kondziolka D, Bernstein M, Resch L, Tator CH, Ross Fleming JF, Venderlinden RG, Schutz H. Significance of hemorrhage into brain tumors: clinicopathologic study. J Neurosurg 1987;67:852–7.
83. Lieu AS, Hwang SL, Howng SL, Chai CY. Brain tumors with hemorrhage. J Formos Med Assoc 1999;98:365–7.
84. Kim DG, Park CK, Paek SH, Choe GY, Gwak HS, Yoo H, Jung HW. Meningioma manifesting intracerebral hemorrhage: a possible mechanism of hemorrhage. Acta Neurochir (Wien) 2000;142:165–8.
85. Asari S, Katayama S, Itoh T, Tsuchida S, Furuta T, Ohmoto T. Neurinomas presenting as spontaneous intratumoral hemorrhage. Neurosurgery 1992;31:406–12.
86. Changaris DG, Powers JM, Perot PL Jr, Hungerford GD, Neal GB. Subependymoma presenting as subarachnoid hemorrhage: case report. J Neurosurg 1981;55:643–5.

87. Weinstein ZR, Downey EF Jr. Spontaneous hemorrhage in medulloblastomas. AJNR Am J Neuroradiol 1983;4:986–8.
88. Atlas SW, Grossman RI, Gomori JM, Hackney DB, Goldberg HI, Zimmerman RA, Bilaniuk LT. Hemorrhagic intracranial malignant neoplasms: spin-echo MR imaging. Radiology 1987;164:71–7.
89. Soffietti R, Ruda R, Mutani R. Management of brain metastases. J Neurol 2002;249:1357–69.
90. Al-Shahi R, Bhattacharya JJ, Currie DG, Papanastassiou V, Ritchie V, Roberts RC, Sellar RJ, Warlow CP, for the SIVMS Collaborators. Scottish Intracranial Vascular Malformation Study (SIVMS): evaluation of methods, ICD-10 coding, and potential sources of bias in a prospective, population-based cohort. Stroke 2003;34:1156–62.
91. Stapf C, Khaw AV, Sciacca RR, Hofmeister C, Schumachen HC, Pile-Spellman J, Mast H, Mohr JP, Hartmann A. Effect of age on clinical and morphological characteristics in patients with brain arteriovenous malformation. Stroke 2003;34:2664–9.
92. Spetzler RF, Martin NA. A proposed grading system for arteriovenous malformations. J Neurosurg 1986;65:476–83.
93. Krings T, Geiprasert S, Luo CB, Bhattacharya JJ, Alvarez H, Lasjaunias P. Segmental neurovascular syndromes in children. Neuroimaging Clin N Am 2007;17:245–58.
94. Unlu E, Temizoz O, Albayram S, Genchellac H, Hamamcioglu MK, Kurt I, Demir MK. Contrast-enhanced MR 3D angiography in the assessment of brain AVMs. Eur J Radiol 2006;60:367–8.
95. Taschner CA, Gieseke J, Le Thuc V, Rachdi H, Reyns N, Gauvrit JY, Leclerc X. Intracranial arteriovenous malformations: time-resolved contrast-enhanced MR angiography with combination of parallel imaging, keyhole acquisition, and k-space sampling techniques at 1.5 T. Radiology 2008;246:871–9.
96. Newton T, Cronqvist S. Involvement of the dural arteries in intracranial arterio-venous malformations. Radiology 1969;90:27–35.
97. Cognard C, Gobin YP, Pierot L, Bailly AL, Houdart E, Casasco A, Chiras J, Merland JJ. Cerebral dural arteriovenous fistulas: clinical and angiographic correlation with a revised classification of venous drainage. Radiology 1995;194:671–80.
98. Waragai M, Takeuchi H, Fukushima T, Haisa T, Yonemitsu T. MRI and SPECT studies of dural arteriovenous fistulas presenting as pure progressive dementia with leukoencephalopathy: a cause of treatable dementia. Eur J Neurol 2006;13:754–9.
99. Van Rooij, Sluzewski M, Beute GN. Dural arteriovenous fistulas with cortical venous drainage: incidence, clinical presentation, and treatment. AJNR Am J Neuroradiol 2007;28:651–5.
100. Meckel S, Maier M, Ruiz DS, Yilmaz H, Scheffler K, Radue EW, Wetzel SG. MR angiography of dural arteriovenous fistulas: diagnosis and follow-up after treatment using a time-resolved 3D contrast-enhanced technique. AJNR Am J Neuroradiol 2007;28:877–84.
101. De Souza JM, Dominques RC, Cruz LC Jr, Domingues FS, Iasbeck T, Gasparetto EL. Susceptibility-weighted imaging for the evaluation of patients with familial cerebral cavernous malformations: a comparison with T2-weighted fast spin-echo and gradient-echo sequences. AJNR Am J Neuroradiol 2008;29:154–8.
102. Zabramski JM, Wascher TM, Spetzler RF, Johnson B, Golfinos J, Drayer BP, Brown B, Rigamonti D, Brown G. The natural history of familial cavernous malformations: results of an ongoing study. J Neurosurg 1994;80:422–32.
103. Cordonnier C, Al-Shahi Salman R, Bhattacharya JJ, Counsell CE, Papanastassiou V, Ritchie V, Roberts RC, Sellar RJ, Warlow C, SIVMS Collaborators. Differences between intracranial vascular malformation types in the characteristics of their presenting hemorrhages: prospective, population-based study. J Neurol Neurosurg Psychiatry 2008;79:47–51.
104. Brunon J, Nuto C. [Natural history of cavernomas of the central nervous system.] Neurochirurgie 2007;53:122–30.
105. Kupersmith MJ, Kalish H, Epstein F, Yu G, Berenstein A, Woo H, Jafar J, Mandel G, De Lara F. Natural history of brainstem cavernous malformations. Neurosurgery 2001;48:47–53.
106. Wilms G, Bleus E, Demaerel P, Marachal G, Plets C, Goffin J, Baert AL. Simultaneous occurrence of developmental venous anomalies and cavernous angiomas. AJNR Am J Neuroradiol 1994;15:1247–54.
107. Lasjaunias P, Burrows P, Planet C. Developmental venous anomalies (DVA): the so-called venous angioma. Neurosurg Rev 1986;9: 233–44.
108. Rigamonti D, Drayer BP, Johnson PC, Hadley MN, Zabramski J, Spetzler RF. The MRI appearance of cavernous malformations (angiomas). J Neurosurg 1987;67:518–24.
109. Latchaw RE, Truwit CL, Heros RC. Commentary: venous angioma, cavernous angioma, and hemorrhage. AJNR Am J Neuroradiol 1994;15: 1255–7.
110. Thron A, Petersen D, Voigt K. Neuroradiologie, Klinik und Pathologie der zerebralen venösen Angiome. Radiologe 1982;22:389–99.
111. Valavanis A, Wellauer M, Yasargil MG. The radiological diagnosis of cerebral venous angioma, cerebral angiography and computed tomography. Neuroradiology 1983;24:193–9.
112. Quinones-Hinojosa A, Gulati M, Singh V, Lawton MT. Spontaneous intracerebral hemorrhage due to coagulation disorders. Neurosurg Focus 2003;15:E3.
113. Ghosh K, Nair AP, Jijina F, Madkaikar M, Shetty S, Mohanty D. Intracranial haemorrhage in severe haemophilia: prevalence and outcome in a developing country. Haemophilia 2005;11:459–62.
114. Cahil DW, Ducker TB. Spontaneous intracerebral hemorrhage. Clin Neurosurg 1982;29:722–79.
115. Boudouresques G, Hauw JJ, Meninger V, Escourolle R, Pertuiset B, Buge A, Lhermitte F, Castaigne P. Hepatic cirrhosis and intracranial hemorrhage: significance of association in 53 pathologic cases. Ann Neurol 1980;8:204–5.
116. Lee HJ, Hinrichs CR. Is coagulopathic liver disease a factor in spontaneous cerebral hemorrhage? J Comput Assist Tomogr 2002;26:69–72.
117. Graus F, Rogers LR, Posner JB. Cerebrovascular complications in patients with cancer. Medicine (Baltimore) 1985;64:16–35.
118. Gugliotta L, Mazucconi MG, Leone G, Mattioli-Belmonte M, Defazio D, Annino L, Tura S, Mandelli F. Incidence of thrombotic complications in adult patients with acute lymphoblastic leukaemia receiving L-asparaginase during induction therapy: a retrospective study. Eur J Haematol 1992;49:63–6.
119. Cowan DH. Effect of alcoholism on hemostasis. Semin Hematol 1980; 17:137–47.
120. Hacke W. Neurologie. Berlin–Heidelberg–New York: Springer, 1999.
121. Wijdicks EF, Jack CR Jr. Intracerebral hemorrhage after fibrinolytic therapy for acute myocardial infarction. Stroke 1993;24:554–7.
122. Kase CS, O´Neal AM, Fisher M, Girgis GN, Ordia JI. Intracranial hemorrhage after use of tissue plasminogen activator for coronary thrombolysis. Ann Intern Med 1990;112:17–21.
123. Kase CS, Pessin MS, Zivin JA, del Zoppo GJ, Furlan AJ, Buckley JW, Snipes RG, LittleJohn JK. Intracranial hemorrhage after coronary thrombolysis with tissue plasminogen activator. Am J Med 1992;92: 384–90.

Address for Correspondence
Jennifer Linn, MD
Department of Neuroradiology
University Hospital Munich
Marchioninistraße 15
81377 München
Germany
Phone (+49/89) 7095-2501, Fax -2509
e-mail: linn@nrad.de